Title
Magnetotail energy dissipation during an auroral substorm.

Journal
Nature physics, 12(12)

ISSN
1745-2473

Authors
Panov, EV
Baumjohann, W
Wolf, RA
et al.

Publication Date
2016-12-01

DOI
10.1038/nphys3879

Peer reviewed

Published in final edited form as:
Nat Phys. 2016 December ; 12(12): 1158–1163. doi:10.1038/nphys3879.

Magnetotail energy dissipation during an auroral substorm

E.V. Panov[1], **W. Baumjohann**[1], **R.A. Wolf**[2], **R. Nakamura**[1], **V. Angelopoulos**[3], **J. M. Weygand**[3], and **M.V. Kubyshkina**[4]

[1]Space Research Institute, Austrian Academy of Sciences, Graz, Austria

[2]Physics and Astronomy Department, Rice University, Houston, Texas, USA

[3]Institute of Geophysics and Planetary Physics, UCLA, Los Angeles, USA

[4]St. Petersburg State University, St. Petersburg, Russian Federation

Abstract

Violent releases of space plasma energy from the Earth's magnetotail during substorms produce strong electric currents and bright aurora. But what modulates these currents and aurora and controls dissipation of the energy released in the ionosphere? Using data from the THEMIS fleet of satellites and ground-based imagers and magnetometers, we show that plasma energy dissipation is controlled by field-aligned currents (FACs) produced and modulated during magnetotail topology change and oscillatory braking of fast plasma jets at 10-14 Earth radii in the nightside magnetosphere. FACs appear in regions where plasma sheet pressure and flux tube volume gradients are non-collinear. Faster tailward expansion of magnetotail dipolarization and subsequent slower inner plasma sheet restretching during substorm expansion and recovery phases cause faster poleward then slower equatorward movement of the substorm aurora. Anharmonic radial plasma oscillations build up displaced current filaments and are responsible for discrete longitudinal auroral arcs that move equatorward at a velocity of about 1km/s. This observed auroral activity appears sufficient to dissipate the released energy.

Introduction

Substorms 1 are magnetospheric disturbances during which energy is released from the tail of the Earth's magnetosphere and injected in the inner magnetosphere and ionosphere. The development of an auroral substorm 2, the visible part of a magnetospheric substorm, has been investigated for the past half century. Multispacecraft observations have revealed that a substorm onset sequence is initiated by magnetotail reconnection 3. Newly reconnected field lines relax their magnetic tension, generating series of earthward flow bursts (bursty bulk

Corresponding author. evgeny.panov@oeaw.ac.at.

Author contributions

E.V.P. developed the research and did the main part of the data analysis; R.A.W. applied analytical thin filament calculations; W.B. and R.A.W. provided theoretical insight into interpretation of the observational data; R.N. and V.A. contributed to the data interpretation and manuscript preparation; J.M.W. applied the spherical elementary currents (SECSs) method to the ground magnetometer data; M.V.K. applied the AM03 model to THEMIS data and traced THEMIS probes' ionospheric footprints; E.V.P. wrote the manuscript, with revisions provided by V.A., W.B., R.N. and R.A.W.; all authors contributed to the discussion of the results and manuscript.

Europe PMC Funders Author Manuscripts

flows or BBFs) 4, 5 that encompass magnetic flux fronts. Because the velocity of newly reconnected magnetic flux in these fronts is substantially lower than that of a flow burst's core, the fronts partly dissipate BBFs' kinetic energy through thermalization and diversion of plasma flows 6, 7. Earthward flow bursts are associated with small auroral expansions 8.

Low entropy BBFs overcome the pressure balance inconsistency 9, 10, enabling magnetic flux transport to the inner magnetosphere. When BBFs deposit flux from the tail to the inner magnetosphere, the magnetotail dipolarizes 11, 12, first around ten Earth radii (R_E), then farther downtail 13, 14. Encounter with and oscillations of the dominant dipolar magnetic field finally brake flow bursts 15, 16, and magnetic flux fronts.

Rapid modification of pressure and entropy distributions in the inner magnetosphere by a slowing flow burst has been suggested to generate an enduring substorm current wedge 17. In addition, azimuthal displacement or bending of field lines in the tail may provide dynamic balancing of the plasma sheet through closure of transient currents in the ionosphere as north-south (meridional) Pedersen currents across the auroral arc 18, 19.

Using simultaneous observations in the near-Earth plasma sheet by five Time History of Events and Macroscale Interactions during Substorms (THEMIS) probes 20, conjugate ground all-sky camera observations from Canada, and magnetometer arrays over North America on 23 March 2009 between 6:00 and 6:40 UT, we investigate the source of dissipation of magnetotail energy released when flow bursts stop. Magnetotail observations were provided by the probes' fluxgate magnetometers (FGM) 21 and their electrostatic analyzer (ESA) particle detectors 22. Ground-based observations of auroral emissions and the ionospheric magnetic field were provided by the All-Sky Imagers (ASI at Snap Lake, Rankin Inlet, and Sanikiluaq) and a dense network of ground magnetometer (MAG) arrays over Greenland and North America 23–25. A fortuitous THEMIS probe configuration in space and with their magnetic footpoints over the aforementioned network of MAGs and ASIs under clear skies, allowed us to unambiguously ascertain the physical connection between ground and space phenomena for an isolated substorm.

23 March 2009 Auroral Substorm

On 23 March 2009 at about 6:04 UT, THEMIS ASIs at Snap Lake (SNAP), Rankin Inlet (RANK), and Sanikiluaq (SNKQ) in Canada started to observe an auroral substorm. Figure a shows a snapshot (at 6:12:30 UT) from the three ASIs. The ASI at SNAP observed a westward traveling surge (a bright bold spot), whereas ASI at RANK observed most of an auroral bulge. The ASI at SNKQ observed the eastward end of an auroral bulge. Note that ASIs at SNAP and SNKQ were contaminated with a non-auroral light (stable white spots at the western edge of ASIs at SNAP and at the northern edge of ASI at SNKQ). A movie (in the auxiliary material) containing all ASI snapshots on 23 March 2009 between 6:00 and 6:40 UT at 3 second cadence shows the dynamics of the two auroral structures throughout the substorm. Between 6:04 and 6:17 UT the auroral bulge expanded northward by more than 7 degrees latitude. After 6:17 UT it started to fade away.

Europe PMC Funders Author Manuscripts

The length and orientation of tiny yellow lines in the snapshot (see zoom-in insert in white rectangle in Figure a) indicate the magnitude and direction of the auroral substructures' local velocities (the lines' origin is always at the edge of an auroral substructure). These velocities were calculated using a computer vision algorithm that solves the optical flow constraint equation. Optical flow is the distribution of apparent velocities of objects in an image (auroral substructures within the ASI snapshots). By estimating optical flow between video frames, one can measure the velocities of objects in the video. We solved the optical flow constraint equation using the Lucas-Kanade method, which divides the original image into smaller sections and assumes a constant velocity in each 26.

Ionospheric Currents

We used magnetometer arrays over Greenland and North America 23–25 and the 2D Spherical Elementary Current Systems (SECSs) method 25, 27 to investigate ionospheric currents on the ground. In this method, the divergence-free elementary current system is expanded at each pole of the grid shown in Figure 2 of 25, allowing derivation of horizontal equivalent ionospheric currents (EICs). Using EICs, we calculated vertical components of the curl of EICs integrated over each grid point area. We refer to the vertical components as SECS scaling factors because the amplitude of each elementary system is scaled (measured in amperes). If the ionospheric conductance gradient is parallel to the electric field direction, the SECS scaling factors are proportional to field-aligned currents (FACs) 27, and the factor of proportionality between FACs and the SECS scaling factors is the Hall-to-Pedersen conductance ratio.

Figure b shows a snapshot of EICs (arrows) and SECS scaling factors (color: upward, reddish; downward, bluish) at 6:12:30 UT (see movie containing all snapshots for 23 March 2009 between 6:00 and 6:40 UT at 1 second cadence in auxiliary material).

The ionospheric current system consists of a pair of vertical (FAC) currents with opposite polarity (reddish and bluish spots in the SECS scaling factors) and a westward electrojet (larger arrows in EICs between the reddish and bluish spots). Between 6:04 and 6:17 UT the ionospheric current area appeared to drastically expand in both the azimuthal and north-south directions. The current maxima moved northward from about 59 degrees latitude to about 63 degrees latitude (close to RANK) between 6:04 and 6:17 UT. By 6:40 UT the ionospheric currents had almost died out. The expansion, northward motion, and dying out of the ionospheric currents thus coincided with the auroral bulge behavior.

Linking an Auroral Substorm with Plasma Sheet Dynamics

The appearance and fading away of the auroral bulge and ionospheric currents reflect the substorm expansion and recovery phases. Assuming that auroral and ionospheric current dynamics originate in the magnetosphere, observations in the plasma sheet may provide a clue about the substorm generation process. The expansion and recovery phases are not one-dimensional (radial) problems. In particular flow divergence in the out-of-plane direction may be responsible for an azimuthal flux transport 28. During the time under discussion, five THEMIS probes (P1-P5) were orbiting inside the near-Earth plasma sheet between -11

and -14 Earth radii (R_E) downtail (Figure a), with their ionospheric footprints in the northern hemisphere near ASI at RANK (see zoom-in insert in black rectangle in Figure b). Such spacecraft location allows us to link plasma sheet and ground ASI and MAG observations near the central part of the auroral bulge.

According to the AM03 model 29, magnetic field line evolution shows that the magnetotail depolarized rapidly between 6:04 and 6:17 UT. After 6:17 UT, magnetic field lines started to stretch tailward. The dipolarization and stretching cover a wide range of x (GSM). As indicated by the black arrow in Figure b, the plasma sheet B_Z magnetic field grew between 6:03 and 6:18 UT (during magnetotail dipolarization), such that the B_Z increase propagated tailward (from $X = -11R_E$ to $X = -14R_E$) at a velocity of $35 km/s$. In contrast, after 6:18 UT (during magnetotail restretching), B_Z decreased earthward at a velocity of $13 km/s$ (from $X = -14R_E$ to $X = -11.5R_E$, black arrow in Figure c).

The auroral electrojet (AL) index (Figure a) reveals substorm expansion (between about 6:03 UT and 6:15 UT) and recovery (after 6:15 UT) phases. Magnetospheric perpendicular currents may divert to parallel because of zero divergence of total (perpendicular plus parallel) current density. For example, when the ions cannot carry all needed perpendicular current in a stronger total field, the divergent (to parallel) diamagnetic perpendicular current is proportional to $\nabla V \times \nabla P$ 30, where P is plasma sheet pressure and V is flux tube volume. The triangular configuration of THEMIS probes in the xy plane (see ionospheric footprints in the northern hemisphere near ASI at RANK, zoom-in insert in black rectangle in Figure b) allowed us to calculate the Z GSM component of $\nabla V \times \nabla P$ in the region between the probes, where V is calculated using formula (6) in 31. The main component contributing to $\nabla V \times \nabla P$ appeared to be $\frac{\partial V}{\partial x}\frac{\partial P}{\partial y}\cdot\frac{\partial V}{\partial x}$ was estimated between THEMIS probes separated along x GSM and confirmed by the AM03 model.

Regions of enhanced $(\nabla V \times \nabla P)_Z$ around the neutral sheet are believed to feed substorm field-aligned currents, as shown by MHD simulations in Figures 4 and 5 in 19. According to these simulations, field-aligned current is oppositely directed on two sides of the flow burst's core. Kinetic particle-in-cell simulations 7 indicate that these currents may be asymmetric due to strong duskward ion flow at the magnetic flux front.

Indeed, Figure b shows that $(\nabla V \times \nabla P)_Z$ grew rapidly during the substorm expansion phase and decreased slowly during the substorm recovery phase. This behavior agrees with development of substorm currents in the ionosphere, Figure e.

The time-integrated average meridional auroral velocity at SNAP, RANK, and SNKQ $\int V_{NS}dt$ (red curve in Figure c) indicates that during the substorm expansion phase, auroral activity moved poleward by about 9 degrees (from about 55 to 64 deg latitude). During the substorm recovery phase, $\int V_{NS}dt$ slowly returned. The ratio between the velocity of tailward expansion of plasma sheet dipolarization ($\approx 35 km/s$, cf. Figure b) and the poleward propagation velocity of the auroral activity ($\approx 1.8 km/s$) is close to the ratio between the velocity of inner plasma sheet restretching ($\approx 13 km/s$, cf. Figure c) and the equatorward propagation velocity of the auroral activity ($\approx 0.7 km/s$). Because of the earthward then

tailward convection of magnetic field lines past the THEMIS probes (Figure a), the geographic latitude of the five THEMIS footprints predicted by the AM-03 model (pink area in Figure c) appeared to partly follow the auroral activity location. In effect, Figures c,d show that a poleward fast-moving bright aurora slows down and dims after the expansion phase, recedes to lower latitudes, then fades away during late substorm recovery phase.

The above observations indicate that non-collinear pressure and flux tube volume gradients in the magnetotail indeed feed the direct part of the ionospheric currents (DC). However, as seen from the ASI observations, auroral activity within the auroral bulge near the maximal ionospheric currents (near RANK) is quite complex (Figure d), and alternating ionospheric currents exist there (Figure e). The amplitudes of the alternating currents are significantly smaller than those of the DC currents; thus, they do not change the direction of the total current.

Aurora During Anharmonic Oscillatory Braking

As predicted by the AM03 model 29, the footprints of THEMIS probes P1 and P2 at the auroral bulge location most of the time. That is, they were located between the red and blue spots of upward and downward ionospheric currents at the westward electrojet current (see movie containing all snapshots of ASI observations at Rankin Inlet on 23 March 2009 between 6:00 and 6:40 UT at 3 second cadence in auxiliary material).

In Figure a we show $\int \delta V_R dt$ – time-integrated oscillations of the radial ion velocity V_R, where δ indicates band pass filtering at periods between 10 and 500 s, and positive V_R means earthward. The location of the oscillating magnetic flux tube with respect to its equilibrium position is indicated by $\int \delta V_R dt$. When the oscillating flux tube was earthward of this position (i.e., when red and green curves in Figure a were above zero), the force acting on it (Figure b) was directed tailward (toward the equilibrium position). During such intervals $(\nabla V \times \nabla P)_Z$ in Figure c exhibited peaks. Hence, the plasma sheet field-aligned current is modulated by the oscillating magnetic flux tube, getting stronger or weaker depending on the location of the oscillating magnetic flux tube with respect to its point of equilibrium. In contrast to the steady (DC) component of $(\nabla V \times \nabla P)_Z$ from Figure b, the alternate (AC) component of $(\nabla V \times \nabla P)_Z$ in Figure c may be partly balanced by inertial currents, agreeing with thin filament simulations. Nonetheless, ground J_{up} (Figure d) still reveals significant (up to 15% of an average magnitude) oscillations.

We correlated space $\int \delta V_R dt$ and ground J_{up} observations. We found that the ionospheric current dynamics lags behind THEMIS observations by about 45s (e.g., a plot of $\int \delta V_R dt$ against J_{up} (not shown) reveals a linear dependence, with the correlation coefficients exceeding 0.9). This time delay is about 15%; the observed oscillation period of $\int \delta V_R dt$ is about 5 minutes. This represents a phase lag of about 1 radian, which is consistent with Figure 25 of 15 for a reasonable level of an average Pedersen conductance in the ionosphere of 3 S.

The intervals of positive $\int \delta V_R dt$ correspond to about 10% – 15% increases in the ionospheric field-aligned currents (Figure d). Every peak in the field-aligned currents

corresponds to enhanced auroral luminosity (Figure e) and velocity (Figure f) of the auroral arcs like the one shown in Figure at RANK (two more arc examples are given in auxiliary material for ground ASI and current observations at 6:17:30 UT and at 6:21:00 UT). The arcs were longitudinally oriented and moved equatorward at a velocity up to 200km/min (with an average value of the order of 50km/min, Figure f). The velocity of the auroral activity (Figure f) peaked when the magnetic flux tube moved earthward from its equilibrium position. Hence, magnetic flux tube oscillations during fast flow braking in the near-Earth plasma sheet modulated the ionospheric current and auroral dynamics during the substorm under study.

Recently, with the help of the thin filament approach 32, the oscillatory flow braking between 6:00 UT and 6:40 UT on 23 March 2009 was suggested to have occurred in an asymmetric potential in which the thin filament oscillations appeared to be anharmonic. Figure shows the theoretical predictions for THEMIS observations on 23 March 2009 around 6:21 UT: phase portrait of a thin filament oscillating anharmonically around its equilibrium position at $X \approx -14R_E$ (a) in the asymmetric potential well U (b). A movie in the auxiliary material shows one period of the thin filament oscillation on 23 March 2009 around 6:21 UT. The force per unit magnetic flux F_X (black arrows in Figure b) acting on the thin filament in its most earthward position (red solid circle at $X \approx -13R_E$) appeared to be about three times larger than F_X in the filament's most tailward position (blue solid circle at $X \approx -16R_E$). Thus, the aurora brightened (field-aligned current enhanced) when the thin filament was earthward of its equilibrium position, and dimmed (field-aligned current depleted) when the thin filament was tailward of its equilibrium position.

Energy consumption rate

According to the above results, when the anharmonically oscillating magnetic flux tube is earthward of its equilibrium position, its interaction with the background plasma sheet is more dramatic: pressure and flux tube volume gradients become enhanced transiently. The plasma sheet currents appear transiently as a result of azimuthal displacement or bending of field lines in the tail and close at the ionospheric side through Pedersen currents across auroral arcs. The westward electrojet current, which is closed to itself, warping the upward and downward field-aligned currents, is the Hall current. Hence, during anharmonic oscillatory flow braking, flow burst kinetic energy may be damped and converted to Joule heating due to Pedersen conductance in the westward electrojet.

The ionospheric Joule heating is a part of the total energy dissipation that occurs during substorms 33, 34. Using an empirical relation between the AE index and the Joule heating 35 one can estimate the Joule heating for both hemispheres during the substorm under study (taking 0.6 GW for 1 nT in the average AE index during the substorm under study of about 50 nT) to be about 3×10^{10}W.

Alternatively, the latitude-integrated precipitation rate near midnight for Kp=2 is about 1024 keV/(s-sr) for each half-hour bin in local time 36. Multiplying by 4 to cover 2 hr in local time, by 2 to include both hemispheres, by π to integrate over a solid angle, and by 1.6×10^{-16} to convert energy units, we get about $4 \times 10^9 W$. Globally, Joule heating comes out to

be of the order of twice the direct loss by precipitation; hence, the total dissipation would be ≈ 8 × 10^9 *W*. This is a little less than the above estimate, which is a reasonable correction due to statistical averaging. Let us compare these estimates with the dissipation rate that can be provided by the observed auroral arcs.

The Alfvenic wave impedance exerted on the current flow by mirror force is $R_W = \frac{\mu_0 R_E L}{\tau_A \Gamma^2} \approx 1.4\Omega,$ where McIlwain number $L \approx 11$, Alfvenic transit time $\tau_A \approx 45s$, and $\Gamma \approx 1.2$ characterizes the high-beta effect on the magnetic field 37. From Figure b we get a current density for ionospheric field-aligned currents of about $j_{e,ion} \approx 100kA/(150km)^2 = 5\mu A/m^2$. Note that the amplitudes of the alternating ionospheric currents are about ten times smaller (10% of the DC currents, Figures e and d). Knowing that the plasma sheet area where the field-aligned currents are generated is equal to or exceeds the area covered by THEMIS probes in the XY GSM plane, about $4R_E^2$, one can obtain the field-aligned current density in the plasma sheet, about $j_e \approx 4nA/m^2$. Knowing that the size of the region with enhanced $(\nabla V \times \nabla P)_Z$ exceeded $3R_E$ (distance between P1,P2 and P3-P5), we find that the energy flux may reach $\dot{W}_{arc} = R_W J_{\parallel,arc}^2 \approx 0.35 W/m^2$, where $J_{\parallel,arc} = j_e \times 3R_E \approx 0.5 A/m.$ Hence, direct energy inflow into the arc with thickness $\omega_{arc} = 50km$ and length $l_{arc} = 1000km$ is $\dot{W}_{arc}\omega_{arc}l_{arc} \approx 1.75 \times 10^{10} W.$

Another energy consumption estimate can be obtained from the potential drop $\Phi_\parallel = \sqrt{\frac{\dot{W}_{arc}}{K}} \approx 35kV,$ where $K = \left(R_W \omega_{arc}^2\right)^{-1} \approx 2.9 \times 10^{-10} S/m^2$ 37. Following empirical expressions for conductivities 38, we estimate the Hall-to-Pedersen conductivity ratio $s = \frac{\Sigma_H}{\Sigma_P} = 0.45 \cdot \Phi_\parallel^{0.85} \approx 9.24$ and the Pedersen conductivity $\Sigma_{P,arc} = 40S \cdot \frac{\Phi_\parallel}{16 + \Phi_\parallel^2} \cdot \sqrt{\frac{\dot{W}_{arc}}{1mW/m^2}} \approx 21.1S.$ Hence, the Cowling conductivity $\Sigma_C = \left(1 + \frac{s^2}{\hat{\alpha}}\right)\Sigma_{P,arc} \approx 1763S,$ where $\hat{\alpha} = 1 + \frac{1}{R_W \Sigma_{P,arc}} \approx 1.034.$ Note that such conductivity levels are found in the brightest substorm auroral elements, such as the surge horn 39. The resulting tangential (westward) electric field in the ionosphere $E_t = \sqrt{\frac{R_W}{\Sigma_C}} J_{\parallel,arc} \approx 14.1 mV/m.$ The total energy consumption in the westward electrojet can be estimated as $\dot{W}_{tot} = 2\Sigma_C E_t^2 \cdot \omega_{arc} \cdot l_{arc} \approx 3.5 \cdot 10^{10} W$ 37, comparable to the above estimates of the direct energy inflow (≈ 1.75 × 10^{10} *W*) and of the Joule heating (between 0.8 × 10^{10}W and 3 × 10^{10}W).

Whereas a substantial part of the magnetotail energy is brought with the magnetic flux 33, 34, only a tenth of the total Joule heating (about 10^9 *W*) can be associated with the oscillating plasma sheet fast flows: in Figures e and d, the amplitudes of the alternating ionospheric currents are about 10% of the DC currents. The fastest flows (observed by P4 at 6:08 UT, not shown here) reached 600*km/s*. Knowing that BBFs occur in very localized

channels up to $3R_E$ wide 11, 33, that the plasma sheet thickness exceeded $3R_E$ (distance between P1 and P5 in the Z_{GSM} direction), and that the radial flow size exceeded $11R_E$ (earthward flow velocity at P4 integrated over 4min braking time between 6:03 UT and 6:07 UT), a minimal flow burst kinetic energy can be estimated as

$W_{fb}=\frac{1}{2}m_p n_p 99 R_E^3 \times (600km/s)^2 \approx 8.1 \times 10^{11} J,$ where m_p is the proton mass, and $n_p \approx 0.1 cm^{-3}$ is the proton number density. Thus, reasonably consistent with the presented THEMIS observations, W_{fb} can be dissipated by five arcs each providing a dissipation rate of $\approx 10^9 W$ over an arc lifetime (Figures e,f) of about three minutes.

Conclusions

The THEMIS space and ground magnetometer and all-sky imager observations analyzed above suggest that substorm current and auroral dynamics are controlled by magnetotail topology change and by produced and modulated during oscillatory braking fast flows at 10-14 Earth radii in the nightside magnetosphere. The auroral bulge appears to map in the flow braking region where the plasma sheet pressure and flux tube volume gradients are non-collinear. Two processes were identified to control the ionospheric current and auroral dynamics during the substorm. (i) A fast (35 km/s) tailward expansion of magnetotail dipolarization and then slower (13 km/s) inner plasma sheet restretching during substorm expansion and recovery phases cause faster (1.7 km/s) poleward, then slower (0.7 km/s) equatorward movement of the substorm auroral bulge. (ii) Plasma sheet parcels, oscillating anharmonically around their equilibrium position and building up stronger pressure and flux tube volume gradients earthward of this position, are responsible for discrete longitudinal auroral arcs within the bulge that move equatorward at a velocity of the order of 1 km/s. The observed auroral activity appears to consume sufficient energy to dissipate the released magnetotail energy.

Data availability

Time History of Events and Macroscale Interactions during Substorms (THEMIS) probes data is available from the Space Physics Data Facility of the Goddard Space Flight Center (http://cdaweb.gsfc.nasa.gov/) All Sky Imager data from THEMIS Mission Data website (http://themis.ssl.berkeley.edu/gbo/display.py); geomagnetic indices from the World Data Center for Geomagnetism, Kyoto (http://wdc.kugi.kyoto-u.ac.jp/); ground magnetometer data from the Canadian Array for Real Time Investigations of Magnetic Activity (http://www.carisma.ca), from Space Physics Data Facility of the Goddard Space Flight Center (http://cdaweb.gsfc.nasa.gov/), and from the SuperMAG consortium (http://supermag.jhuapl.edu). Upon request the authors will attempt to provide all other data supporting this study.

Supplementary Material

Refer to Web version on PubMed Central for supplementary material.

Acknowledgments

We acknowledge NASA contract NAS5-02099 for use of data from the THEMIS Mission, and specifically, for the use of FGM data supported through the German Ministry for Economy and Technology and the German Center for Aviation and Space (DLR) under contract 50 OC 0302. For the GBO/ASIs, we acknowledge S. Mende and E. Donovan, NASA contract NAS5-02099 and the CSA for logistical support in fielding and data retrieval from the GBO stations. The authors gratefully acknowledge AUTUMN, CANMOS, CARISMA, DTU, GIMA, MACCS, McMAC, STEP, THEMIS, and USGS for the use of ground-based magnetic field data over Greenland and North America. The work of M.V.K. was supported by RFBR grant 16-05-00470. The work of E.V.P. and R.N. was partly supported by the Austrian Science Fund (FWF) I429-N16 and by the Seventh Framework European Commission Programme (FP7, project 269198 Geoplasmas). The authors thank Olaf Amm for helping with ionospheric currents calculations, J. Hohl for helping with editing, Karl-Heinz Glaßmeier, Olga Panova, Anatoli A. Petrukovich, Victor A. Sergeev, and Frank R. Toffoletto for insightful discussions.

References and Notes

1. McPherron RL. Magnetospheric substorms. Reviews of Geophysics and Space Physics. 1979; 17:657–681.
2. Akasofu S-I. Auroral substorms as an electrical discharge phenomenon. Progress in Earth and Planetary Science. 2015; 2:1–21.
3. Angelopoulos V, et al. Tail Reconnection Triggering Substorm Onset. Science. 2008; 321:931–935. [PubMed: 18653845]
4. Baumjohann W, Paschmann G, Luehr H. Characteristics of high-speed ion flows in the plasma sheet. J Geophys Res. 1990; 95:3801–3809.
5. Angelopoulos V, et al. Statistical characteristics of bursty bulk flow events. J Geophys Res. 1994; 99:21257–21280.
6. Angelopoulos V, et al. Electromagnetic Energy Conversion at Reconnection Fronts. Science. 2013; 341:1478–1482. [PubMed: 24072917]
7. Drake JF, Swisdak M, Cassak PA, Phan TD. On the 3-D structure and dissipation of reconnection-driven flow bursts. Geophys Res Lett. 2014; 41:3710–3716. 1401.7056.
8. Nakamura R, et al. Earthward flow bursts, auroral streamers, and small expansions. J Geophys Res. 2001; 106:10791–10802.
9. Pontius DH Jr, Wolf RA. Transient flux tubes in the terrestrial magnetosphere. Geophys Res Lett. 1990; 17:49–52.
10. Baumjohann W. Modes of convection in the magnetotail. Phys Plasmas. 2002; 9:3665–3667.
11. Nakamura R, et al. Plasma flow and magnetic field characteristics near the midtail neutral sheet. J Geophys Res. 1994; 99:23591–23601.
12. Schödel R, Nakamura R, Baumjohann W, Mukai T. Rapid flux transport and plasma sheet reconfiguration. J Geophys Res. 2001; 106:8381–8390.
13. Baumjohann W, et al. Substorm dipolarization and recovery. J Geophys Res. 1999; 104:24995–25000.
14. Birn J, Nakamura R, Panov EV, Hesse M. Bursty bulk flows and dipolarization in MHD simulations of magnetotail reconnection. J Geophys Res. 2011; 116:A01210.
15. Wolf RA, Chen CX, Toffoletto FR. Thin filament simulations for Earth's plasma sheet: Interchange oscillations. J Geophys Res. 2012; 117:A02215.
16. Panov EV, et al. Oscillatory flow braking in the magnetotail: THEMIS statistics. Geophys Res Lett. 2013; 40:2505–2510.
17. Sergeev VA, Chernyaev IA, Angelopoulos V, Runov AV, Nakamura R. Stopping flow bursts and their role in the generation of the substorm current wedge. Geophys Res Lett. 2014; 41:1106–1112.
18. Birn J, Hesse M, Haerendel G, Baumjohann W, Shiokawa K. Flow braking and the substorm current wedge. J Geophys Res. 1999; 104:19895–19904.
19. Kepko L, et al. Substorm Current Wedge Revisited. Space Sci Rev. 2015; 190:1–46.
20. Angelopoulos V. The THEMIS Mission. Space Sci Rev. 2008; 141:5–34.
21. Auster HU, et al. The THEMIS Fluxgate Magnetometer. Space Sci Rev. 2008; 141:235–264.

22. McFadden JP, et al. The THEMIS ESA plasma instrument and in-flight calibration. Space Sci Rev. 2008; 141:277–302.
23. Mende SB, et al. The THEMIS array of ground-based observatories for the study of auroral substorms. Space Sci Rev. 2008; 141:357–387.
24. Mann IR, et al. The Upgraded CARISMA Magnetometer Array in the THEMIS Era. Space Sci Rev. 2008; 141:413–451.
25. Weygand JM, et al. Application and validation of the spherical elementary currents systems technique for deriving ionospheric equivalent currents with the North American and Greenland ground magnetometer arrays. J Geophys Res. 2011; 116:A03305.
26. Barron J, Fleet DJ, Beauchemin SS. Performance of Optical Flow Techniques. International Journal of Computer Vision. 1994; 12:43–77.
27. Amm O, Kauristie K. Ionospheric Signatures Of Bursty Bulk Flows. Surv Geophys. 2002; 23:1–32.
28. Hsieh M-S, Otto A. Thin current sheet formation in response to the loading and the depletion of magnetic flux during the substorm growth phase. J Geophys Res. 2015; 120:4264–4278.
29. Kubyshkina M, et al. Time-dependent magnetospheric configuration and breakup mapping during a substorm. J Geophys Res. 2011; 116:A00I27.
30. Vasyliunas, VM. Mathematical Models of Magnetospheric Convection and Its Coupling to the Ionosphere. Particles and Field in the Magnetosphere, vol. 17 of Astrophysics and Space Science Library. McCormack, BM.; Renzini, A., editors. 1970. p. 60-71.
31. Wolf RA, et al. Estimating local plasma sheet $PV^{5/3}$ from single-spacecraft measurements. J Geophys Res. 2006; 111:A12218.
32. Panov EV, Wolf RA, Kubyshkina M, Baumjohann W, Nakamura R. Anharmonic oscillatory flow braking in the Earth's magnetotail. Geophys Res Lett. 2015; 42:3700–3706.
33. Angelopoulos V, et al. Multipoint analysis of a bursty bulk flow event on April 11, 1985. J Geophys Res. 1996; 101:4967–4989.
34. Miyashita Y, et al. A statistical study of energy release and transport midway between the magnetic reconnection and initial dipolarization regions in the near-Earth magnetotail associated with substorm expansion onsets. J Geophys Res. 2012; 117:A11214.
35. Baumjohann W, Kamide Y. Hemispherical Joule heating and the AE indices. J Geophys Res. 1984; 89:383–388.
36. Hardy DA, Gussenhoven MS, Holeman E. A statistical model of auroral electron precipitation. J Geophys Res. 1985; 90:4229–4248.
37. Haerendel G. Poleward arcs of the auroral oval during substorms and the inner edge of the plasma sheet. J Geophys, Res. 2009; 114:A06214.
38. Robinson RM, Vondrak RR, Miller K, Dabbs T, Hardy D. On calculating ionospheric conductances from the flux and energy of precipitating electrons. J Geophys Res. 1987; 92:2565–2569.
39. Gjerloev JW, Hoffman RA. Height-integrated conductivity in auroral substorms. 1. Data. J Geophys Res. 2000; 105:215–226.

Europe PMC Funders Author Manuscripts

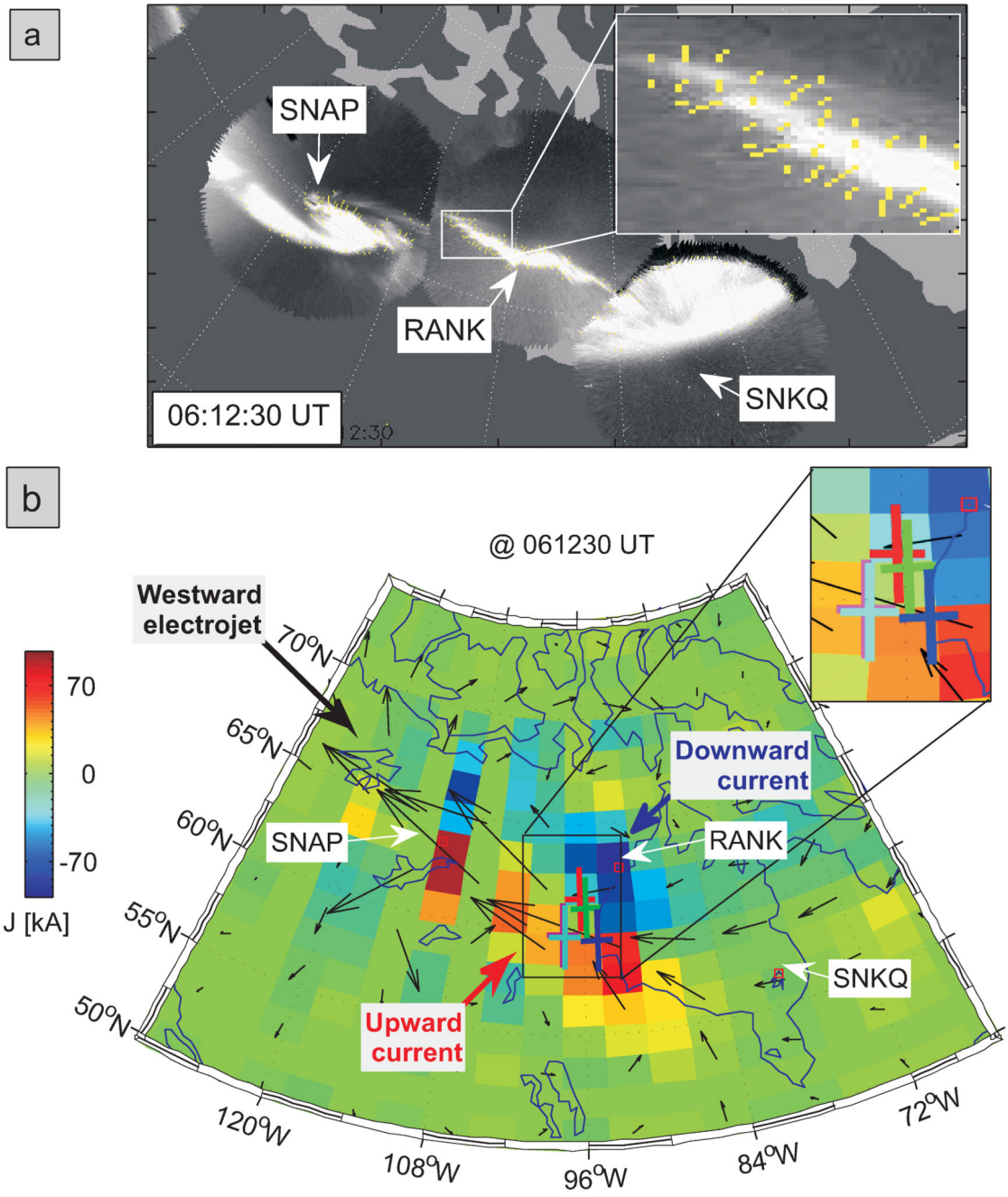

Figure 1. Ground observations of aurora and electric currents

(a) Snapshot from three ASIs at Snap Lake (SNAP), Rankin Inlet (RANK), and Sanikiluaq (SNKQ) at 6:12:30 UT. Tiny yellow lines show local velocity of auroral substructures. (b) Current system structure on the ground: snapshot of EICs (arrows) and the SECS scaling factors (color: upward in reddish, and downward in bluish) at 6:12:30 UT, calculated using ground-based magnetometer array data. The footprints of the five THEMIS probes as predicted by the AM03 model are denoted by overplotted crosses (red for P1, green for P2, blue for P3, cyan for P4, and magenta for P5; see also zoom-in).

Europe PMC Funders Author Manuscripts

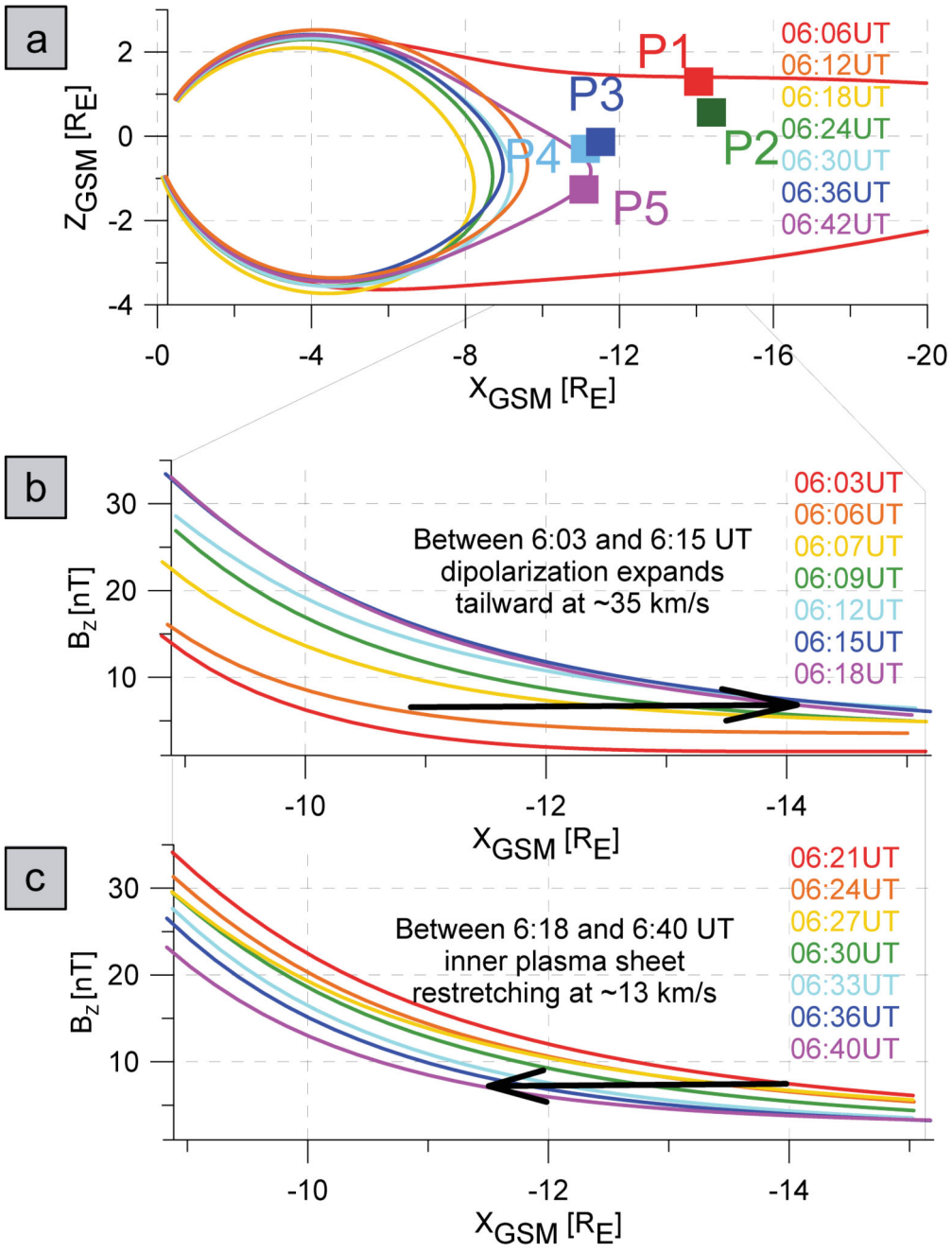

Figure 2. AM 03 model predictions of the magnetotail development near THEMIS probes

(a) Locations of THEMIS probes P1-P5 on 23 March 2009 at 6:12 UT projected onto the noon meridian GSM plane. Evolution of the magnetic field lines between 6:02 and 6:42 UT and of the B_Z magnetic field component (b) for 6:03 and 6:18 UT and (c) for 6:21 and 6:40 UT according to the AM03 model are overplotted (see legends for color coding).

Europe PMC Funders Author Manuscripts

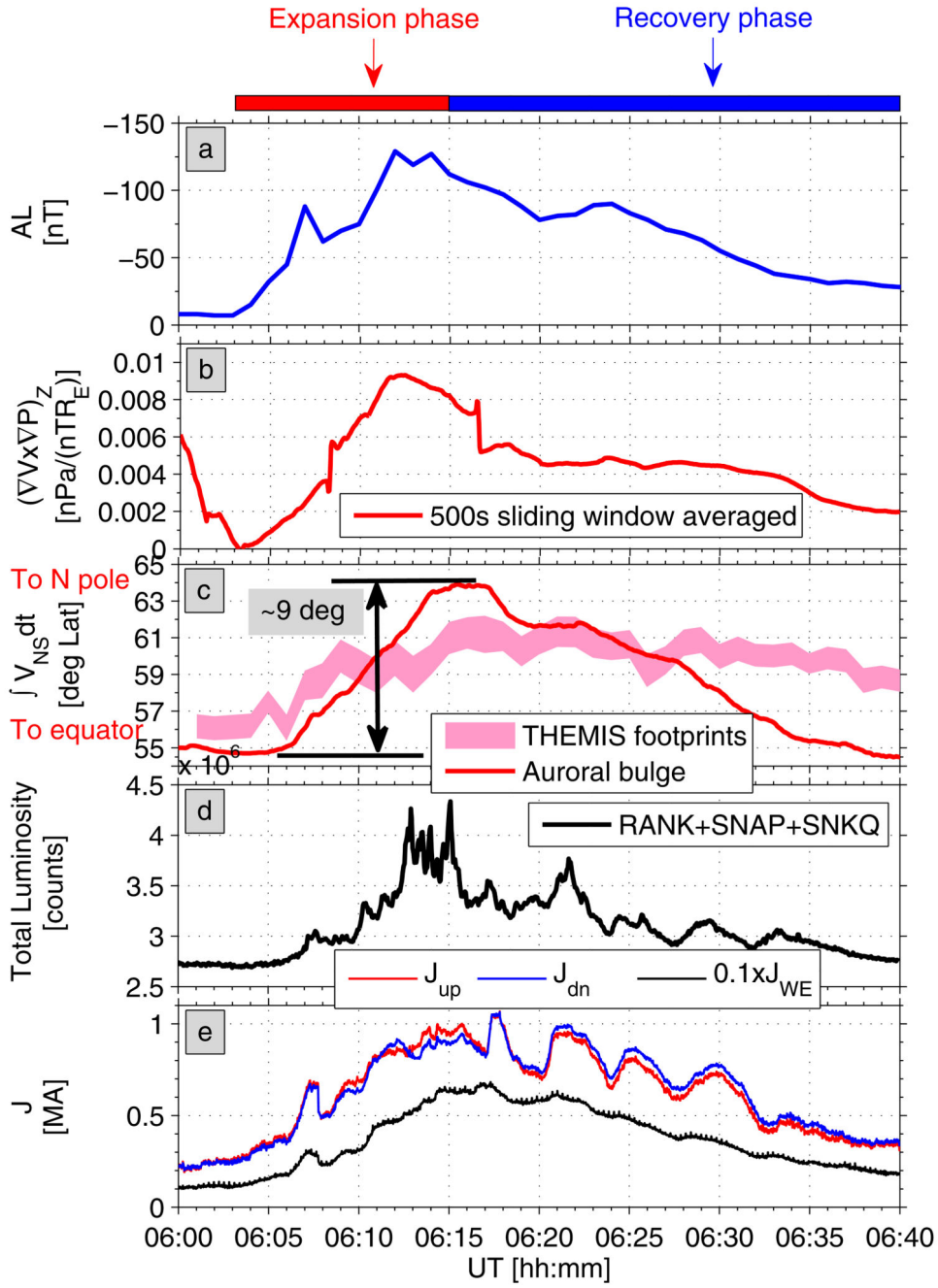

Figure 3. Overview of substorm parameters during substorm expansion and recovery phases

(a) AL auroral electrojet index. (b) $(\nabla V \times \nabla P)_Z$, where P is plasma sheet pressure and flux tube volume V is calculated using formula (6) in 31. (c) Time-integrated average meridional auroral velocity at SNAP, RANK, and SNKQ (red curve), and geographic latitudes covered by the five THEMIS footprints, as predicted by the AM-03 model (pink area). (d) Total auroral luminosity from SNAP, RANK, and SNKQ. (e) Total upward and downward SECS scaling factors and horizontal EICs (see legend) on 23 March 2009 between 6:00 and 6:40 UT.

Europe PMC Funders Author Manuscripts

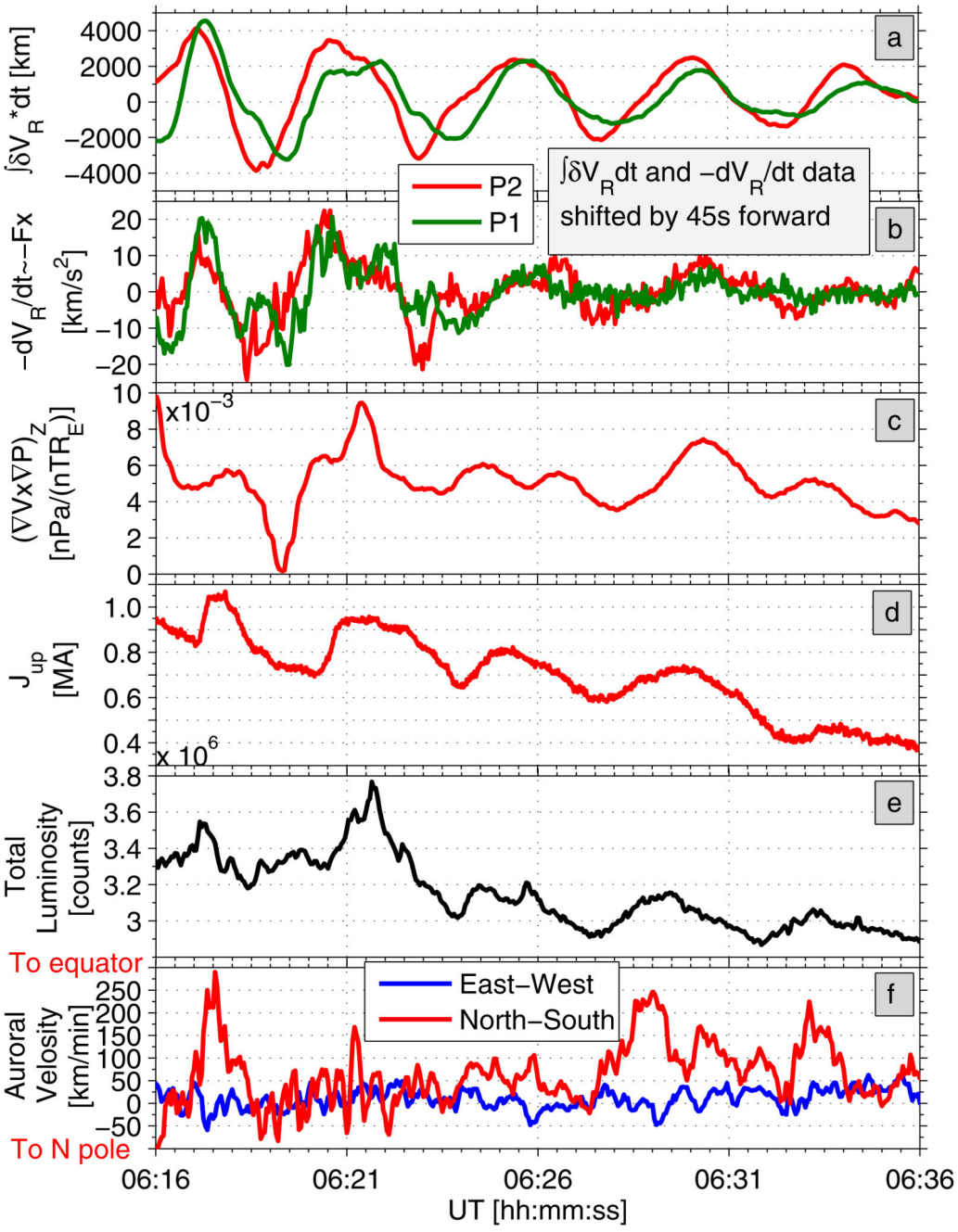

Figure 4. THEMIS space and ground observations on 23 March 2009 between 6:16 UT and 6:36 UT

(a) Time-integrated oscillations of radial ion velocity V_R at P1 (red) and P2 (green), (b) time derivative of oscillations in V_R at P1 (red) and P2 (green), (c) $(\nabla V \times \nabla P)_Z$, where P is plasma sheet pressure and flux tube volume V is calculated using formula (6) in 31, (d) total upward J_{up} SECS scaling factors around Rankin Inlet, (d) total auroral luminosity from SNAP, RANK, and SNKQ, (e) meridional (red) and longitudinal (blue) auroral velocity components. Auroral speed and velocity components were averaged over field of view of RANK.

Europe PMC Funders Author Manuscripts

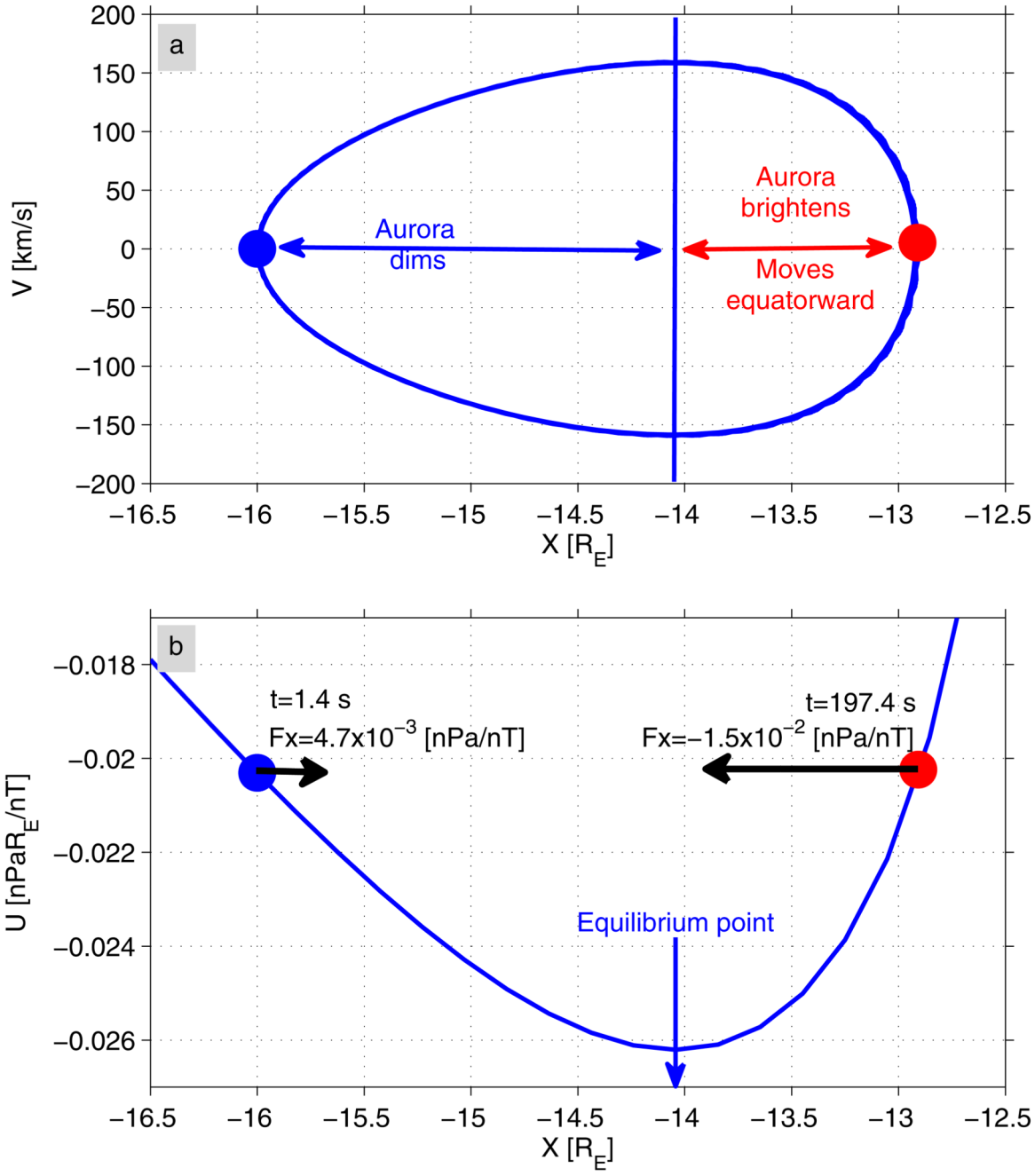

Figure 5. Theoretical predictions for THEMIS observations on 23 March 2009 around 6:21 UT

phase portrait of a thin filament oscillating anharmonically around its equilibrium position at $X \approx -14R_E$ (a) in the asymmetric potential well U (b). Force per unit magnetic flux F_X is given in the most tailward ($X \approx -16R_E$) and most earthward ($X \approx -13R_E$) positions reached by the thin filament.